Parabolic dielectric reflector for extreme on-chip spot-size conversion with broad bandwidth

LAUREANO MORENO-POZAS[1,*], MIGUEL BARONA-RUIZ[1], ROBERT HALIR[1], JOSÉ DE-OLIVA-RUBIO[1], JORGE RIVAS-FERNÁNDEZ[1], IÑIGO MOLINA-FERNÁNDEZ[1], J. GONZALO WANGÜEMERT-PÉREZ[1], AND ALEJANDRO ORTEGA-MOÑUX[1]

[1] *Photonics & RF Research Lab., Telecommunication Research Institute (TELMA), Universidad de Málaga, Louis Pasteur 35, 29010, Málaga, Spain.*
[*] *laureano.moreno@uma.es*

Compiled October 30, 2024

Spot-size converters are key for efficient coupling of light between waveguides of different sizes. While adiabatic tapers are well suited for small size differences, they become impractically long for expansion factors around ×100 which are often required when coupling integrated waveguides and free-space beams. Evanescent couplers and bragg deflectors can be used in this scenario, but their operation is inherently limited in bandwidth. Here we propose a solution based on a parabolic dielectric interface that couples light from a 0.5 µm-wide waveguide to a 285 µm-wide waveguide, i.e. an expansion factor of ×570. We experimentally demonstrate an unprecedented bandwidth of more than 380 nm with insertion losses below 0.35 dB. We furthermore provide analytical expressions for the design of such parabolic spot-size-converters for arbitrary expansion factors.

http://dx.doi.org/10.1364/ao.XX.XXXXXX

Silicon photonics is a burgeoning technology for optical communications due to its compatibility with complementary metal-oxide-semiconductor (CMOS) processes, which enables the integration of photonic circuits and microelectronics [1–3]. Spot-size converters (SSC) are key components in such photonic systems as they enable efficient coupling between waveguides of different sizes. In particular, SSCs are often used to feed gratings that couple light to fibers [4], or project it into free-space [5–8]. The latter requieres spot-size expansions to hundreds of micrometers to achieve beams with Rayleigh ranges of the order of centimeters [7]. This is achieved by first using a SSC to expand light on-chip in the lateral direction from a single-mode waveguide to the desired width (typically exceeding 100 µm). The resulting expanded mode then feeds a weak grating that gradually couples the light into free-space, thereby providing the desired longitudinal expansion [5]. In this scenario traditional adiabatic tapering cannot provide the required spot size conversion within reasonable footprints and therefore other solutions are preferred in the literature.

Silicon-nitride (SiN) platforms have leveraged evanescent couplers to feed very large gratings [5–7, 9]. However, in these SSCs the propagating angle of the expanded modes varies with wavelength. This is due to variations in the effective index of the mode traveling through evanescently coupled waveguide and leads to oblique incidence on the grating which causes spurious changes in its radiation angle [5]. In the Silicon-on-insulator (SOI) SSC designs based on Bragg deflectors [10–12] have been presented. However, due to their resonant nature these SSCs are also strongly wavelength dependent. Integrated lenses could potentially overcome these bandwidth limitations, but so far designs have been limited to MFD below 40 µm [13, 14].

An interesting approach based on parabolic dielectric reflectors in SOI was presented in [15]. Based on total internal reflection, an expansion from a single mode waveguide to a MFD of 7 µm was demonstarted, with losses below 0.25 dB in a bandwidth of 100 nm. Here, we show, for the first time, how this approach can be exploited for extreme SSCs, as illustrated in Fig. 1. We derive analytical expressions to i) minimize power loss due to imperfect total internal reflection , and (ii) minimize the area of the device. Using this approach we demonstrate coupling from a the fundamental TE mode of a 0.5 µm wide waveguide to the fundamental mode of a 285 µm wide waveguide, with measured losses below 0.35 dB across a bandwidth exceeding 380 nm, limited by the measurement setup. In terms of the bandwidth × expansion figure of merit, this is an 98-fold improvement with respect to the state-of-the-art.

The geometry of the SSC is depicted in Fig. 1(a) and (b), expanding the fundamental TE mode from a $W_{\text{in}} = 0.5$ µm wide photonic wire with a thickness of 220 nm to an ouput waveguide with a width of W_{out}. Both the top and bottom claddings are silicon dioxide, with a refractive index $n_c = 1.44$ at $\lambda_0 = 1.55$ µm. Its operation is analogous to an offset parabolic antenna, with the dielectric interface acting as reflector with a focal length F. The parabolic interface follows the equation [15]

$$y = \frac{x^2}{4F}. \tag{1}$$

The input waveguide at port $P1$ is adiabatically tapered over a length L_t to a width W_{ap}, as shown in Fig. 1b. Light then travels through a free propagation region, experiencing diffraction with a divergence angle θ_{div}, until it reflects at the parabolic interface and eventually reaches the output port with width W_{out}.

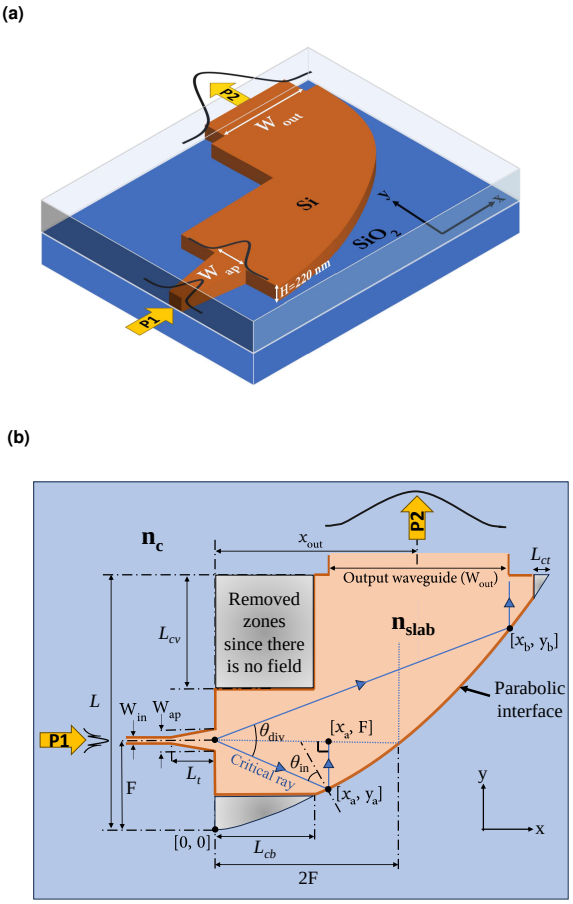

Fig. 1. Device geometry in (a) 3D and (b) 2D. Light diffracts from the aperture of width W_{ap} and then impinges the parabolic interface to create a light beam that travels towards the output waveguide.

The aperture size W_{ap} governs the divergence angle as

$$\theta_{div} = \frac{2.35\lambda_0}{W_{ap} n_{slab}}, \tag{2}$$

where λ_0 represents the vacuum wavelength and n_{slab} denotes the effective index of the free space region ($n_{slab} = 2.85$ for TE polarization at $\lambda_0 = 1.55$ µm). Our definition of the divergence angle corresponds to $\times 1.3$ its classical value [16], thereby encapsulating more than 95% of the transmitted power within the resultant light cone, depicted in Fig. 1b with its extreme rays in blue. This is crucial to ensure low-loss operation. The focal length F is then given by [15]

$$F = \frac{W_{out}}{4\tan(\theta_{div}/2)}. \tag{3}$$

The extreme rays in blue in Fig. 1b impinge on the parabolic interface at points $[x_a, y_a]$ and $[x_b, y_b]$ with coordinates [15]

$$x_{a,b} = 2F\left[\mp\tan\left(\frac{\theta_{div}}{2}\right) + \sqrt{\tan^2\left(\frac{\theta_{div}}{2}\right)+1}\right], \tag{4}$$

and $y_{a,b}$ given by eq. (1).

To minimize device the area, we need to maximize the divergence angle or, equivalently, from eq. (2), minimize W_{ap}. However, W_{ap} should not be too small since we must meet total internal reflection (TIR) at the parabolic interface for all the rays coming from the aperture, i.e. $\theta_{in} \geq \arcsin(n_c/n_{slab})$ [17]. The most restrictive ray is the one that impinges the parabolic interface at $[x_a, y_a]$ since it does so with the smallest angle θ_{in}^{min}. We refer to it as critical ray in Fig. 1b. From the rectangular triangle conformed by the points $[x_a, y_a]$, $[0, F]$ and $[x_a, F]$ and depicted in Fig 1b, we arrive at the following expression for θ_{in}^{min}:

$$\theta_{in}^{min} = \pi/4 - \theta_{div}/4. \tag{5}$$

Since the angle θ_{in}^{min} must meet the TIR condition [17], we find that

$$\pi/4 - \theta_{div}/4 > \arcsin\left(\frac{n_c}{n_{slab}}\right), \tag{6}$$

which requires that $\arcsin(n_c/n_{slab}) < \pi/4$ since $\theta_{div} > 0$, i.e. $n_c/n_{slab} < 1/\sqrt{2} \approx 0.71$. For TE polarization $n_c/n_{slab} = 1.44/2.85 \approx 0.51$, so this condition is always fulfilled. Substituting the divergence angle θ_{div} from (2) into (6) we find:

$$W_{ap} > \frac{2.35\lambda_0}{n_{slab}\left(\pi - 4\arcsin\left(n_c/n_{slab}\right)\right)}. \tag{7}$$

From Eq. (7), we find that for the standard SOI platform with a silicon thickness of 220 nm and silica in the top and bottom-cladding ($n_c = 1.444$), we have $n_{slab} = 2.85$ for TE polarization at $\lambda_0 = 1.55$ µm, which yields $W_{ap} > 1.3$ µm . Moreover, it is clear that the device cannot work for TM polarization with a silicon thickness of 220 nm, since in this case $n_{slab} = 2.05$, which results in $W_{ap} > 126$ µm to meet the TIR condition.

Our design methodology relies on first choosing the aperture size W_{ap} to minimize the area of the device, employing the TIR condition proposed in eq. (7) with a small margin of 0.2 µm, i.e. $W_{ap} = 1.5$ µm. Note that even using a slightly larger aperture $W_{ap} = 2$ µm would already result in 30 % larger device footprint. The footprint can be further reduced by 8% when selecting $W_{ap} = 1.3$ µm, although this comes with a 0.4 dB increase in insertion losses (IL) in the proposed design. In this work, insertion losses are defined as $\mathrm{IL[dB]} = -10\log_{10}(P_2/P_1)$, with P_2 the power in the fundamental TE mode of the output port , and P_1 the power of the fundamental TE mode launched into the input port.

Subsequently, we set the focal length F using equations (2) and (3). With these dimensions, aided by Fig. 1b, the parabolic reflector is defined when selecting $L = 1.2y_b$, with y_b the ordinal coordinate of the upper extreme point in the parabolic interface represented in Fig. 1b, with coordinates $[x_b, y_b]$ given by eq. (1) and eq. (4). The factor 1.2 leaves a small margin of 20% on top of the light cone. The rest of additional equations for delineating the zones where there is no field are given by

$$L_{cb} = 0.8x_a, \tag{8}$$

$$L_{ct} = \sqrt{1.2Fy_b} - \sqrt{Fy_b}, \tag{9}$$

$$L_{cv} = 1.2y_b - 2F - \frac{(0.8x_a)^2}{4F}, \tag{10}$$

where the factors 0.8 and 1.2 give margins of ±20% around the light cone. When removing those margins we degrade insertion losses in 0.1 dB.

Notably, this design process is entirely analytical. In the proposed design, we have optimized the output waveguide center by shifting it +3 µm from the analytical position $x_{out} = 2F = 315$ µm, which yields a 0.2 dB improvement of the insertion losses.

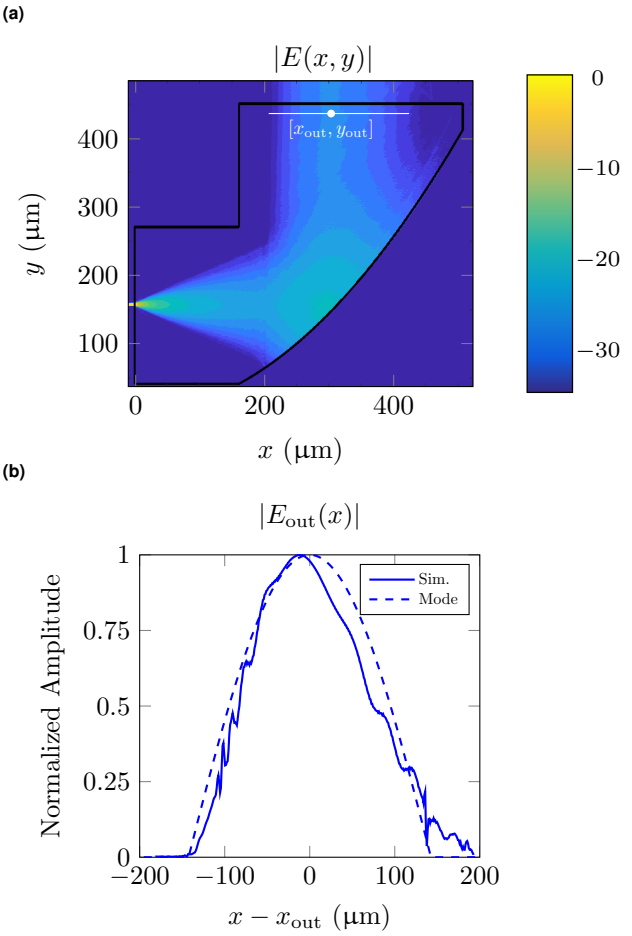

Fig. 2. 2.5-FDTD simulation of the field in the extreme SSC. (a) Propagation of the field and (b) Amplitude of the field at $y = y_{out}$. In dashed lines we represent the amplitude of the mode of the output waveguide.

We confirm the analytical design procedure by designing a parabolic SSC with $W_{out} = 285$ μm, which corresponds to an expansion factor W_{out}/W_{in} of ×570, and whose dimensions are given in Table 1. We perform simulations with Lumerical's 2.5-dimensional finite-difference time-domain (FDTD) method. Upon inspection of the device propagation of field in Fig. 2a, we confirm that the removed corners exhibit a field drop below −35 dB (dark blue). We also present the magnitude of the field at $y = y_{out}$ in Fig. 2b, which yields IL = 0.3 dB at $\lambda_0 = 1.55$ μm. These results are obtained for an FDTD step size of 10 nm and the time step given by the Courant formula. This fine mesh is required to avoid errors in the dispersion relation that affect the phase of the lightwave [18]. Indeed, the convergence analysis shown in Fig. 3 reveals that larger mesh-sizes fail to accurately describe the ultra-low losses of the device. Decreasing the step size below 10 nm might be desirable but is limited by practical tradeoffs of memory requirements and simulation time.

The extreme SSC with the dimensions specified in Table 1 was fabricated with Applied Nantool's single etch process, for 220 nm SOI, with a 2 μm thick buried oxide layer [19]. A 100 keV electron beam was employed to pattern the resist, and the structures were transferred into the silicon layer through reactive ion etching. A 2.2 μm-thick oxide layer was then deposited on

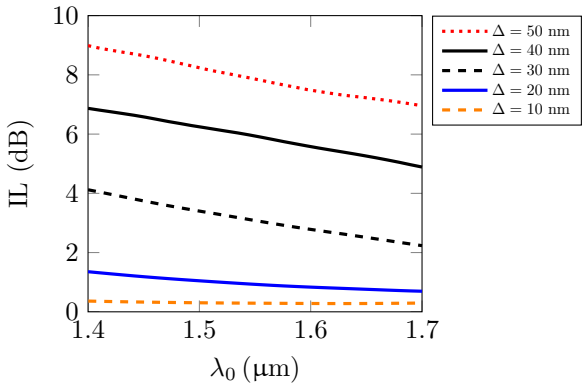

Fig. 3. Insertion loss for different mesh sizes $\Delta_x = \Delta_y = \Delta$ for the extreme SSC as a function of wavelength, where measurement is given in orange solid line.

Table 1. Design values for the extreme parabolic SSC[a]

W_{in}	L_t	W_{ap}	W_{out}	F	L	x_{out}	L_{cb}	L_{ct}	L_{cv}
0.5	10	1.5	285	157.5	455	318	203	23	74.6

[a] All values are in micrometers.

top using chemical vapor deposition. SEM micrographs of the device are presented in Fig. 4a before deposition of the upper cladding. The chip incorporates several flavours of the device with varying positions of the input waveguide (varying F in Fig. 1b) in ±100nm and ±200nm, to compensate possible fabricating errors in the parabolic interface.

For testing, pairs of identical SSCs were connected back-to-back as shown schematically in the inset of Fig. 4b, so that insertion losses can be determined with a simple fibre-to-fibre measurement. To cover the 1.26 μm to 1.64 μm wavelength range, light from three tunable lasers (Agilent 81600B series, options 072 and 160, and Santec TSL-770-P-480640-P-F-AP-00-1) is coupled into the chip from a polarization-maintaining fibre though a subwavelength edge coupler [20]. The fiber is positioned on a rotational stage and combined with a Glan–Thompson polarizer at the output, enabling us to control the polarization coupled into the chip. At the chip's output, light is focused onto a photodetector (Newport 818-IR) using a microscope objective lens. The transmission spectrum is recorded by varying the tunable laser's wavelength while monitoring the output power.

Measurements of the insertion losses of a single SSC are given in Fig. 4b. They are obtained by measuring the transmission spectrum of two identical SSCs in the back-to-back configuration shown in the inset of Fig. 4b, normalizing to a reference waveguide to cancel out fiber-to-chip coupling losses, and dividing the resulting spectrum, expressed in dB, by two. Our measurements demonstrate that IL < 0.35 dB from 1.26 to 1.64 μm. Our device exhibits an increase of ×26 in expansion and ×3.8 in bandwidth compared to previous parabolic reflectors [15]. A detailed comparison of our design with other existing wide-band devices in the literature is provided in Table 2, where the figure of merit (FoM) is given by the product of the 1-dB bandwidth in μm and the magnification. This comparison highlights that our extreme SSC is state-of-the-art and presents an excellent solution for creating SSCs with very large expansion ratios.

In conclusion, we have demonstrated that parabolic dielectric

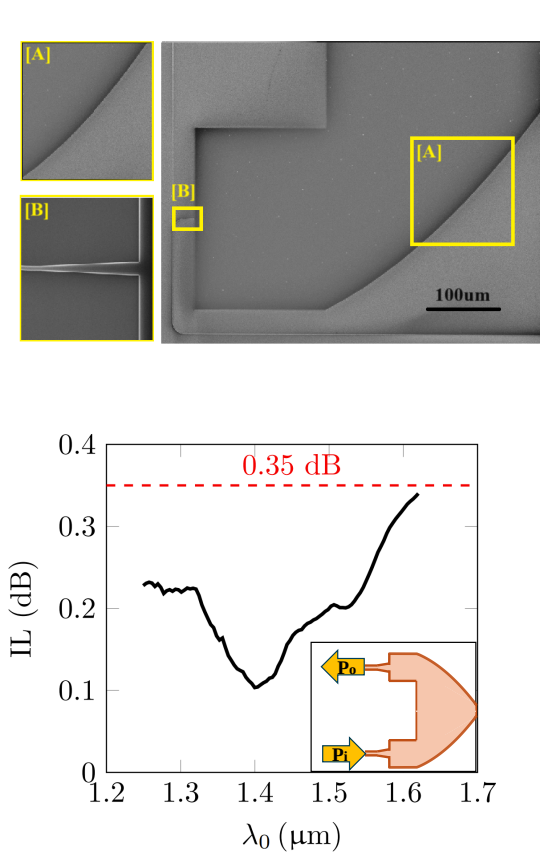

Fig. 4. Fabricated extreme parabolic SSC. (a) SEM of the device with details and (b) Measured insertion losses of a single SSC. Insertion losses are measured with the transmission spectrum of the back-to-back configuration shown in the inset.

interfaces are a good solution when large spot-size conversions are required. Specifically, we have tackled the conversion of the fundamental TE mode from a 0.5 μm SOI waveguide to a waveguide with width up to 285 μm, or equivalently a mode with a MFD up to 200 μm, i.e. SSC with a magnification factor up to ×570. Key to our result is the TIR condition in Eq. (7), which provides a straightforward way to achieve ultra-low losses, below 0.35 dB over an inherently broad bandwith (380 nm). The proposed design can be entirely analytical, when fixing the output waveguide center $x_{out} = 2F$, with no significant cost in terms of IL. This may be of interest to design a Process Design Kit (PDK). This design represents a promising advancement towards efficient spot-size conversion for different integrated photonic applications, irrespective of the working wavelength.

Funding. We acknowledge funding through project TED2021-130400B-I00/AEI/10.13039/501100011033/ Unión Europea NextGenerationEU/PRTR and project PDC2023-145833-I00/ Ministerio de Ciencia, Innovación y Universidades.

Disclosures. The authors declare no conflicts of interest.

Data availability. Data underlying the results presented in this paper are not publicly available at this time but may be obtained from the authors upon reasonable request.

Table 2. Performance of some state-of-the art SSC in SOI[a]

Ref.	W_{in}	W_{out}	IL(dB)	BW_{1dB}(nm)	platform	FoM
[11, 12]	0.5	57	0.3	N/A	SOI	N/A
[13]	0.5	15	0.6	130	SOI	3.9
[14]	0.5	10	0.8	220	SOI	4.4
[15]	0.45	10	0.15	> 100	SOI	> 2.2
This work	0.5	285	0.23	> 380	SOI	> 216.6

[a] All dimensions are in microns unless otherwise specified. Insertion losses are given at $\lambda_0 = 1.55$ μm. Bandwidth is measured as the wavelength range where IL are below 1 dB.

REFERENCES

1. S. Shekhar, W. Bogaerts, L. Chrostowski, *et al.*, Nat. Commun. **15**, 751 (2024).
2. X. Chen, M. M. Milosevic, S. Stanković, *et al.*, Proc. IEEE **106**, 2101 (2018).
3. L. Rinaldi, F. Camponeschi, and A. Bogoni, J. Light. Technol. (2023).
4. R. Halir, P. Cheben, S. Janz, *et al.*, Opt. letters **34**, 1408 (2009).
5. S. Kim, D. A. Westly, B. J. Roxworthy, *et al.*, Light. Sci. & Appl. **7**, 72 (2018).
6. A. Yulaev, W. Zhu, C. Zhang, *et al.*, ACS photonics **6**, 2902 (2019).
7. A. Yulaev, D. A. Westly, and V. A. Aksyuk, ACS photonics **10**, 945 (2022).
8. X. Ding, Z. Wang, G. Hu, *et al.*, PhotoniX **1**, 1 (2020).
9. C. Ropp, W. Zhu, A. Yulaev, *et al.*, Light. Sci. & Appl. **12**, 83 (2023).
10. A. Hadij-ElHouati, P. Cheben, A. Ortega-Moñux, *et al.*, Opt. Express **27**, 33180 (2019).
11. A. Hadij-ElHouati, P. Cheben, A. Ortega-Moñux, *et al.*, Opt. Lett. **46**, 2409 (2021).
12. P. Ginel-Moreno, A. Hadij-ElHouati, A. Sánchez-Postigo, *et al.*, Laser & Photonics Rev. **16**, 2200164 (2022).
13. J. M. Luque-González, R. Halir, J. G. Wangüemert-Pérez, *et al.*, Laser & Photonics Rev. **13**, 1900172 (2019).
14. Y. Zhang, Y. He, H. Wang, *et al.*, ACS Photonics **8**, 202 (2020).
15. H. Xu, Y. Qin, G. Hu, and H. K. Tsang, Opt. Lett. **48**, 327 (2023).
16. B. E. Saleh and M. C. Teich, *Fundamentals of photonics* (John Wiley & Sons, 2019).
17. S. J. Orfanidis, *Electromagnetic waves and antennas* (Chapter 7, Rutgers University New Brunswick, NJ, 2002).
18. A. Taflove, S. C. Hagness, and M. Piket-May, The Electr. Eng. Handb. **3**, 15 (2005).
19. Applied Nanotools Inc., "Applied Nanotools NanoSOI Fabrication Service," .
20. P. Cheben, J. H. Schmid, S. Wang, *et al.*, Opt. express **23**, 22553 (2015).

FULL REFERENCES

1. S. Shekhar, W. Bogaerts, L. Chrostowski, *et al.*, "Roadmapping the next generation of silicon photonics," Nat. Commun. **15**, 751 (2024).
2. X. Chen, M. M. Milosevic, S. Stanković, *et al.*, "The emergence of silicon photonics as a flexible technology platform," Proc. IEEE **106**, 2101–2116 (2018).
3. L. Rinaldi, F. Camponeschi, and A. Bogoni, "Space-grade analogue and digital photonics for satellite communications in europe," J. Light. Technol. (2023).
4. R. Halir, P. Cheben, S. Janz, *et al.*, "Waveguide grating coupler with subwavelength microstructures," Opt. letters **34**, 1408–1410 (2009).
5. S. Kim, D. A. Westly, B. J. Roxworthy, *et al.*, "Photonic waveguide to free-space gaussian beam extreme mode converter," Light. Sci. & Appl. **7**, 72 (2018).
6. A. Yulaev, W. Zhu, C. Zhang, *et al.*, "Metasurface-integrated photonic platform for versatile free-space beam projection with polarization control," ACS photonics **6**, 2902–2909 (2019).
7. A. Yulaev, D. A. Westly, and V. A. Aksyuk, "Surface-normal free-space beam projection via slow-light standing-wave resonance photonic gratings," ACS photonics **10**, 945–952 (2022).
8. X. Ding, Z. Wang, G. Hu, *et al.*, "Metasurface holographic image projection based on mathematical properties of Fourier transform," PhotoniX **1**, 1–12 (2020).
9. C. Ropp, W. Zhu, A. Yulaev, *et al.*, "Integrating planar photonics for multi-beam generation and atomic clock packaging on chip," Light. Sci. & Appl. **12**, 83 (2023).
10. A. Hadij-ElHouati, P. Cheben, A. Ortega-Moñux, *et al.*, "Distributed bragg deflector coupler for on-chip shaping of optical beams," Opt. Express **27**, 33180–33193 (2019).
11. A. Hadij-ElHouati, P. Cheben, A. Ortega-Moñux, *et al.*, "High-efficiency conversion from waveguide mode to an on-chip beam using a metamaterial engineered bragg deflector," Opt. Lett. **46**, 2409–2412 (2021).
12. P. Ginel-Moreno, A. Hadij-ElHouati, A. Sánchez-Postigo, *et al.*, "On-chip metamaterial antenna array with distributed bragg deflector for generation of collimated steerable beams," Laser & Photonics Rev. **16**, 2200164 (2022).
13. J. M. Luque-González, R. Halir, J. G. Wangüemert-Pérez, *et al.*, "An ultracompact GRIN-lens-based spot size converter using subwavelength grating metamaterials," Laser & Photonics Rev. **13**, 1900172 (2019).
14. Y. Zhang, Y. He, H. Wang, *et al.*, "Ultra-broadband mode size converter using on-chip metamaterial-based luneburg lens," ACS Photonics **8**, 202–208 (2020).
15. H. Xu, Y. Qin, G. Hu, and H. K. Tsang, "Compact integrated mode-size converter using a broadband ultralow-loss parabolic-mirror collimator," Opt. Lett. **48**, 327–330 (2023).
16. B. E. Saleh and M. C. Teich, *Fundamentals of photonics* (John Wiley & Sons, 2019).
17. S. J. Orfanidis, *Electromagnetic waves and antennas* (Chapter 7, Rutgers University New Brunswick, NJ, 2002).
18. A. Taflove, S. C. Hagness, and M. Piket-May, "Computational electromagnetics: the finite-difference time-domain method," The Electr. Eng. Handb. **3**, 15 (2005).
19. Applied Nanotools Inc., "Applied Nanotools NanoSOI Fabrication Service," .
20. P. Cheben, J. H. Schmid, S. Wang, *et al.*, "Broadband polarization independent nanophotonic coupler for silicon waveguides with ultra-high efficiency," Opt. express **23**, 22553–22563 (2015).